本計劃主要目的是研究垂直共振腔雷射(VCSEL)所形成之圖案。第一年之工作主要是 VCSEL 之製作及光學量測系統之建立，特別是低溫光學量測系統，以下就針對第一年已完成之工作做一簡單之報告說明。

工作進度說明：

(一)　VCSEL 之研製

在 VCSEL 方面，本實驗室已有多年之經驗，但此計劃主要是製作可產生高階橫模之大面積 VCSEL，與先前之小面積 VCSEL 完全不同。為產生高階橫模大面積 VCSEL 必須在橫向有極好之 optical confinement 並在電流注射上做不同之考量與設計。第一年之工作中已製作出正方形、圓形與橢圓形等形狀之大面積 VCSEL， 由特殊之光學 confinement 設計，初步已可看到極為高階之橫模。

(二)　光學系統

第一年之另一重點為光學橫模之圖案量測，因高階橫模之發散角極大，故 VCSEL 近場之量測極為困難。本實驗室目前已克服大角度發散之問題，初步已可量測到發散角達 100° 左右之 VCSEL 近場。另外，在低溫下 VCSEL 會轉換至更高階之橫模，故低溫光學系統，特別是大

角度 VCSEL 在低溫下之光學量測，是第一年投入最多之工作。原先使用一台 closed-cycle 低溫系統，該系統量測遠場較無問題，但近場量測時則因振動過大，無法取得清晰圖像。故已提前採購一台 continuous flow 之低溫系統，目前已安裝完畢，遠場量測初步已無問題。近場量測則尚在設計及安裝相關光學配件。預計很快即可取得穩定之近場圖像。

經費變更說明：

本計劃目前進展順利，初步取得之結果已陸續發表於 Phys. Rev. Letts, Phys. Rev. E。但因 continuous flow 系統購入後，取代先前使用之 closed-cycle 系統(振動過大)，故 LHe 之使用遠超過先前計劃所編列之經費，為使計劃能繼續完成，故申請增加 LHe 費用 60 萬元，另外，新增博士生及碩士生各一人，請同意增加人事費 20 萬元。

參考文獻：

1. K.F. Huang, Y.F. Chen, H.C. Lai, and Y.P. Lan, “Observation of the Wave Function of a Quantum Billiard from the Transverse Patterns of Vertical Cavity Surface Emitting Lasers”, Phys. Rev. Lett. 89, 224102 (2002).
2. Y.F. Chen, K.F. Huang, H.C. Lai, and Y.P. Lan, “Observation of Vector Vortex Lattices in Polarization States of an Isotropic Microcavity Laser”, Phys. Rev. Lett. 90, 053904 (2003).

Observation of the Wave Function of a Quantum Billiard from the Transverse Patterns of Vertical Cavity Surface Emitting Lasers

K. F. Huang, Y. F. Chen,* and H. C. Lai
Department of Electrophysics, National Chiao Tung University, Hsinchu, Taiwan, Republic of China

Y. P. Lan
Institute of Electro-Optical Engineering, National Chiao Tung University, Hsinchu, Taiwan, Republic of China
(Received 26 April 2002; published 11 November 2002)

We demonstrate experimentally that the near-field and far-field transverse patterns of a large aperture vertical cavity surface emitting laser (VCSEL) can be successfully interpreted as a two-dimensional (2D) billiard system. It is found that the near-field and far-field transverse patterns of a large aperture VCSEL evidently represent the coordinate-space and momentum-space wave functions of a 2D quantum billiard, respectively. The result of this paper suggests that large aperture VCSELs are potentially appropriate physical systems for the wave-function study in quantum problems.

DOI: 10.1103/PhysRevLett.89.224102 PACS numbers: 05.45.Mt, 42.55.Sa, 42.60.Jf

Vertical cavity surface emitting lasers (VCSELs) have become of considerable interest for short-range data communications and sensor applications [1]. Of scientific interest, VCSELs inherently emit in single-longitudinal mode due to their extremely short cavity length, but large aperture devices can exhibit a complex transverse mode structure. The transverse mode pattern and the polarization instabilities in VCSELs have been the main interests in the past few years [2–7]. Hegarty *et al.* [8] reported interesting transverse mode patterns from oxide-confined square-shaped VCSELs with larger aperture. Their experimental results revealed that a wave incident upon the current-guiding oxide boundary would undergo total internal reflection because of large index discontinuities between the oxide layer and the surrounding semiconductor material. Namely, VCSELs can be considered as a planar waveguide with a dominant wave vector along the vertical direction. Because of the analogy between the Schrodinger and Helmholtz equations [9], it is essentially feasible to use the oxide-confined VCSEL cavities, such as microwave cavities [10,11], to represent quantum mechanical potential wells. In this case, the transverse patterns can reveal the probability density of the corresponding wave functions to the two-dimensional quantum billiards. However, such a correspondence has not been established as yet because the thermal effects usually result in a complex refraction-index distribution to distort the VCSEL planoplanar resonators [6].

In this Letter, we experimentally demonstrate that, when the thermal effects are reduced by cooling the device at the temperature below 10 °C, the near-field and far-field transverse patterns of a large aperture VCSEL evidently represent the coordinate-space and momentum-space wave functions of a 2D quantum billiard, respectively. The satisfactory correspondence implies that VCSELs are appropriate devices for the study of the behavior of the wave functions in quantum billiard problems. Since VCSELs, in general, can be fabricated for any two-dimensional shape, this versatility makes these devices extremely flexible to explore a great deal of interesting physics.

In this investigation, we fabricate square-shaped VCSELs with large aperture and measure near-field and far-field patterns of the transverse mode. The size of the oxide aperture is $40 \times 40\ \mu m^2$. The device structure of these oxide-confined VCSELs and the methods used to measure the far-field and near-field patterns are similar to those described by Ref. [8]. Experimental results show that the transverse patterns of VCSELs can be certainly divided into two regimes of low-divergence and high-divergence emissions. Hereafter, we will concentrate on the high-divergence emission, which appears only at reduced temperature and near threshold operation. It is expected the thermal-lensing effect will switch the device into the low-divergence regime because the joule heating induces a temperature rise across the device cross section. Typically, high-divergence patterns are very symmetric and those of low divergence are more irregular. Therefore it is easy to differentiate the regimes in which the lasers are being operated.

We first controlled the device at the temperature of 10 °C. As shown in Fig. 1, the near-field pattern of the device was found to be a bouncing-ball scar that is similar to the result of Ref. [8], except that the order is higher. It can be seen that the observed bouncing-ball scar is not perfectly periodic but contains dislocations to show some wavy structure. Even so, the laser beam was measured to be linearly polarized. As the device was cooled at the temperature around 0 °C, the near-field pattern changed dramatically, as shown in Fig. 2. It can be seen that the near-field intensity apparently was highly concentrated along the trajectory of a diamond-shaped classical orbit. Although this diamond "scar" has been discussed extensively in the wave functions of ballistic quantum dots

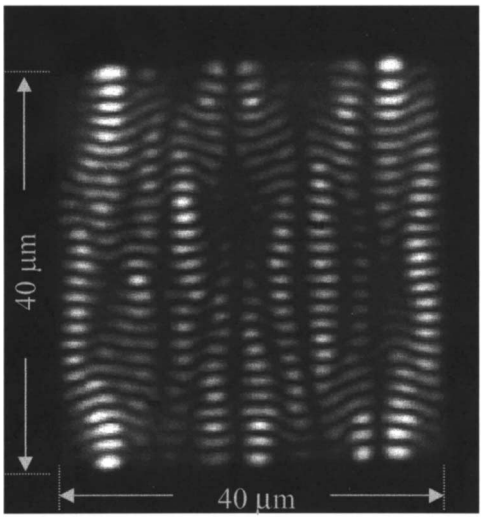

FIG. 1. The experimental result for the near-field pattern of the VCSEL device near the lasing threshold. The device was operated at the temperature 10 °C.

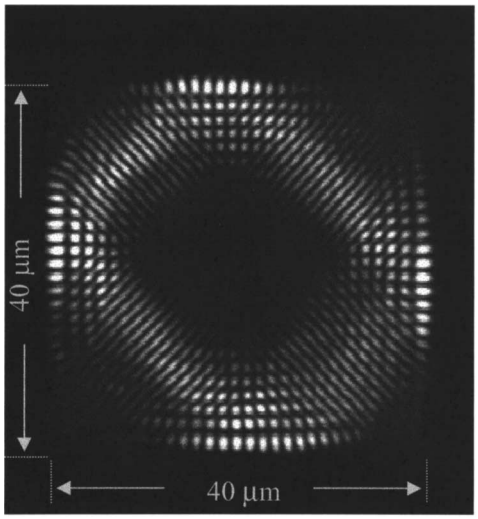

FIG. 2. The experimental result for the near-field pattern of the VCSEL device near the lasing threshold. The device was operated at the temperature 0 °C

[12–14], it is the first time to observe this interesting pattern from a laser transverse pattern. The specific wave scars confirm the fact that the oxide-confined VCSELs can be considered as a planar waveguide.

In order to understand the observed transverse patterns, it is helpful to simplify the VCSEL structure first. We consider the large aperture VCSEL to be a very narrow square-shaped three-dimensional resonator with embedded gain material. The two distributed feedback reflectors (DBR) were separated by nearly one wavelength and the square-shaped oxide aperture defined the lateral billiard boundary. The wave vectors can be decomposed into k_z and k_t, where k_z is the wave-vector component along the direction of vertical emission and k_t is the transverse wave-vector component. Since the vertical dimension is designed to be nearly one wavelength, k_z is the dominating component in the emission wave vector. The lateral boundary has a dimension of $40 \times 40\ \mu\text{m}^2$; consequently, the transverse k_t is much smaller than k_z. The lateral oxide boundary can be considered as rigid walls with infinite potentials since the photons will experience total reflection at the lateral oxide walls due to a large k_z component and a relatively small transverse component k_t. Furthermore, since the mirrors in VCSELs are DBRs, they can be considered as plane mirrors with no curvature. The photons can be treated as particles confined in a boundary with infinite potential and zero potential inside the square. Vertical emission in the z direction can be considered to be the coupling of the resonance fields inside the cavity to the outside medium through the top DBR. Therefore, the phasor amplitude of the emission field distribution $E(x, y, z)$ is conveniently given by $E(x, y, z) = \psi(x, y)e^{-jk_z z}$. After separating the z component in the wave equation, we are left with a two-dimensional Helmholtz equation: $(\nabla_t^2 + k_t^2)\psi(x, y) = 0$. Here, ∇_t^2 means the Laplacian operator operating on the coordinates in the transverse plane and $\psi(x, y)$ is a scalar wave function that describes the transverse profile of the laser. The solutions to the Helmholtz equation with total internal reflection boundaries are equivalent to the solutions of the 2D Schrodinger equation with hard wall boundaries [$\psi(x, y) = 0$ at the boundary] of the same geometry. This analogy has been exploited most successfully in microwave cavities and scarred eigenfunctions of a chaotic billiard have been demonstrated [10,11]. The wave functions for the 2D quantum billiards are also important understanding the behavior of mesoscopic structures, and will be crucial for the design of nanoscale electronic devices [12–14].

It is well known that the solution to a perfect square billiard can be obtained by separation of variables. However, this subtle solution definitely cannot account for the present observed pattern. It is self-evident that the perfect square billiard is quite rare in most of the real physical problems. In real VCSEL devices, the square aperture is fabricated first by etching a square mesa and then oxidizes the AlAs layer to form the oxide boundary. Process induced deformation is unavoidable, and therefore a perfect square billiard is not appropriate for the simulation. In order to simulate the square billiard formed by the oxide aperture, we modify the square by rounding off the corners. With the rounded off square boundary, the Helmholtz equation can no longer be solved by the method of separation of variables. We use a numerical method called expansion method [15] to solve the equation. Because of symmetry breaking, the eigenfunctions obtained are much more interesting than those of the perfect square billiard. For low order solutions, the patterns are similar to those of the perfect square billiard. However, the higher order eigenfunctions are drastically different in structure and very rich patterns appear. It is of surprising interest that some of the solutions display the

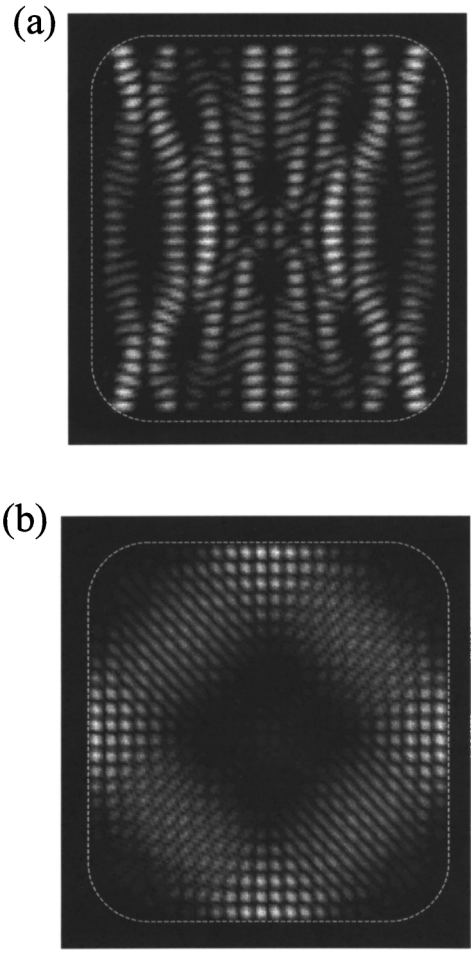

FIG. 3. The calculated wave functions of the square billiards modified by rounding off the corners. (a) and (b) are similar to the observed near-field patterns in Figs. 1 and 2, respectively. The dashed lines indicate the boundary of the simulation.

distorted bouncing-ball and diamond-shaped scars similar to the experimental results. Figure 3 shows two of the calculated eigenfunctions that are similar to the observed near-field patterns in Figs. 1 and 2. Note that the present modified square billiards always have the high-order eigenfunctions demonstrating the distorted bouncing-ball and diamond-shaped scars, almost irrelevant to the degree of how much the corners are rounded off.

It is worthwhile to mention that Nöckel and Stone [16] have designed stadium-shaped microcavity lasers and demonstrated high power directional emission in the midinfrared wavelength based on some chaotic two-dimensional billiard dynamics. However, due to the geometrical structure of the laser, only edge emission was allowed in these deformed microdisk lasers. Therefore, a comparison between the experimentally determined far-field pattern and simulation was limited for only one dimension. The near-field pattern was not measured because high-resolution midinfrared detection was not possible.

The optical far-field intensity essentially is the spatial 2D Fourier transform (FT) of the near-field pattern, while the FT of the coordinate-space wave function corresponds to the momentum-space representation in the quantum mechanics. Recently, Delande and Sornette [17] have calculated the acoustic radiation from a stadium-shaped membrane by applying FT to the eigenfunctions. Similar calculations focusing on the momentum representation of the wave functions were also reported by Bäcker and Schubert [18]. Both theoretical papers suggested that momentum distribution of a two-dimensional quantum billiard is actually experimentally observable and such information can provide a more comprehensive understanding to the billiard system. Therefore, it is consequentially meaningful to measure the far-field pattern for the VCSEL devices. Figure 4 shows the experimental observation of the far-field pattern corresponding to the diamond-shaped wave function in Fig. 2. It can be clearly seen that the far-field pattern exhibited some strong intensity lotus flower structure at the corners of the square and some weak stripes connecting the lotus structure. This far-field pattern is consistent with the near-field

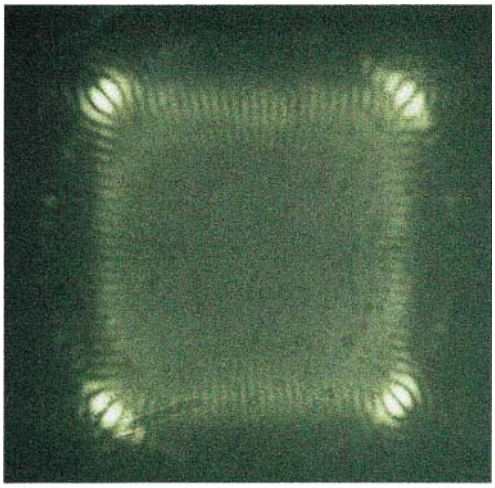

FIG. 4 (color). The experimental result for the far-field pattern corresponding to the near-field pattern in Fig. 2.

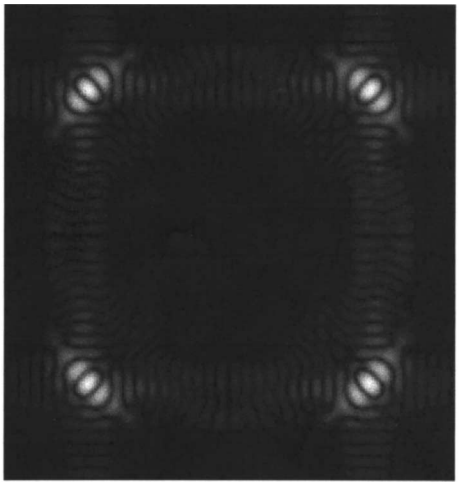

FIG. 5. The calculated momentum-space wave function corresponding to the coordinate-space wave function in Fig. 3(b).

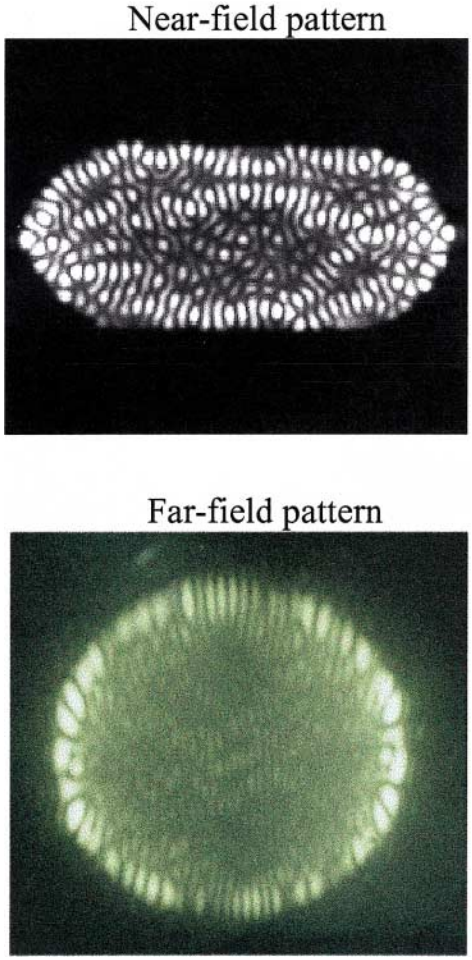

FIG. 6 (color). Experimental results of the near-field and far-field patterns for the VCSEL device with a stadium-shaped boundary.

diamond-shaped scar that apparently was concentrated along the trajectory traced by a particle bouncing off the neighboring walls of the square. Figure 5 shows the momentum-space wave function of the theoretical diamond-shaped scar shown in Fig. 3. The good agreement between experimental results and theoretical calculations confirms our physical analysis and validates the present theoretical model.

Finally, it is worthwhile to clarify that the present interpretation is based on the assumption that the influence of carrier dynamics on the transverse pattern near threshold is negligible. To further justify this assumption, we fabricated the devices with a shape of Bunimovich stadium boundary and measured the near-field and far-field intensities. As shown in Fig. 6, the near-field intensity displays a scarred pattern and the far-field intensity resembles the calculated results of Refs. [17,18] in appearance. The boundary-shape dependence of the VCSEL patterns confirms the present interpretation.

In conclusion, we have observed unique near- and far-field transverse patterns in large aperture VCSELs. A two-dimensional quantum billiard model is utilized to explain the experiments. It turns out the square billiard with minor modification is adequate to simulate the real device. Rounding off the corners certainly breaks the symmetry and introduces coupling of the two originally independent variables. This symmetry breaking makes the solution of the high-order eigenfunctions much more interesting as they display highly graphical patterns. The observed near-field pattern in the transverse mode apparently can be interpreted as from these solutions. Furthermore, the corresponding far-field patterns can also be explained by the momentum-space wave functions in the billiard. The result of this paper also suggests that large aperture VCSELs are potentially appropriate physical systems for the quantum chaos study.

The authors gratefully acknowledge various VCSEL devices from TrueLight Corporation. The authors also thank the National Science Council for their financial support of this research under Contract No. NSC-91-2112-M-009-030.

*Corresponding author.
Electronic address: yfchen@cc.nctu.edu.tw

[1] W.W. Chow, K.D. Choquette, M. Hagerot-Crowford, K.L. Lear, and G.R. Hadley, IEEE J. Quantum Electron. **33**, 1810 (1997).
[2] M. San Miguel, Q. Feng, and J.V. Molony, Phys. Rev. A **52**, 1728 (1995).
[3] M.P. van Exter, M.B. Willemsen, and J.P. Woerdman, Phys. Rev. A **58**, 4191 (1998).
[4] S. Balle, E. Tolkachova, M. San Miguel, J.R. Tredicce, J. Martin-Regalado, and A. Gahl, Opt. Lett. **24**, 1121 (1999).
[5] M. Brambilla, L.A. Lugiato, F. Prati, L. Spinell, and W.J. Firth, Phys. Rev. Lett. **79**, 2042 (1997).
[6] T. Ackeman, S. Barland, M. Cara, S. Balle, J.R. Tredicce, R. Jäger, M. Grabherr, M. Miller, and K.J. Ebeling, J. Opt. B **2**, 406 (2000).
[7] C. Degen, I. Fischer, and W. Elsäßer, Opt. Ex. **5**, 38 (1999).
[8] S.P. Hegarty, G. Huyet, J.G. McInerney, and K.D. Choquette, Phys. Rev. Lett. **82**, 1434 (1999).
[9] J.J. Hupert and G. Ott, Am. J. Phys. **34**, 260 (1966).
[10] S. Sridhar, Phys. Rev. Lett. **67**, 785 (1991).
[11] J. Stein and H.J. Stöckmann, Phys. Rev. Lett. **68**, 2867 (1992).
[12] R. Akis, D.K. Ferry, and J.P. Bird, Phys. Rev. Lett. **79**, 123 (1997).
[13] R. Akis, D.K. Ferry, J.P. bird, and D. Vasileska, Phys. Rev. B **60**, 2680 (1999).
[14] Y.H. Kim, M. Barth, H.J. Stöckmann, and J.P. Bird, Phys. Rev. B **65**, 165317 (2002).
[15] D.L. Kaufman, I. Kosztin, and K. Schulten, Am. J. Phys. **67**, 133 (1999).
[16] J.U. Nöckel and A.D. Stone, Nature (London) **385**, 45 (1997).
[17] D. Delande and D. Sornette, J. Acoust. Soc. Am. **101**, 1793 (1997).
[18] A. Bäcker and R. Schubert, J. Phys. A **32**, 4795 (1999).

Observation of Vector Vortex Lattices in Polarization States of an Isotropic Microcavity Laser

Y. F. Chen,* K. F. Huang, and H. C. Lai
Department of Electrophysics, National Chiao Tung University, Hsinchu, Taiwan, Republic of China

Y. P. Lan
Institute of Electro-Optical Engineering, National Chiao Tung University, Hsinchu, Taiwan, Republic of China
(Received 27 August 2002; published 6 February 2003)

We experimentally investigate the formation of a vector polarization pattern from an isotropic microcavity laser. It is found that the orthogonal components of the observed pattern are localized on the geometrical rays. The connection between eigenfunctions and geometrical rays is analytically constructed by using the SU(2) coherent states. With the analytical function form, the observed vector pattern is completely reconstructed and the vector vortex lattice is apparent.

DOI: 10.1103/PhysRevLett.90.053904 PACS numbers: 42.25.Ja, 03.65.–w, 42.55.Sa, 42.60.Jf

Vortices appear in various aspects of modern physics such as vortex lattices in superconductors, quantum Hall effects, and Bose-Einstein gases [1–3]. In a light wave, the phase singularity of the complex scalar field forms an optical vortex [4–6]. Both single optical vortex and optical vortex lattices have been experimentally observed in lasers [7,8]. In addition to scalar vortices, paraxial optical fields can exhibit vector vortices associated with a space-dependent polarization [9–11]. The single vector vortex has been experimentally observed in CO_2 lasers [12] and in vertical cavity surface emitting lasers (VCSELs) [13]. However, the vector vortex lattice thus far has not been observed in lasers. The difficulty of forming a vector vortex lattice is that the laser cavity needs to be a large Fresnel number and high-level isotropic.

Recently, Hegarty *et al.* [14] reported interesting transverse mode patterns from oxide-confined square shaped VCSELs with large Fresnel number. Their experimental results reveal that a wave incident upon the oxide boundary would undergo total internal reflection because of large index discontinuities between the oxide layer and the surrounding semiconductor material. In this work, we present an experimental observation of vector vortex lattices in a square shaped VCSEL with large aperture. Experimental results reveal that the transverse mode of the square shaped VCSEL can display a vector polarization pattern associated with the geometrical ray when the thermal effects and the cavity anisotropies are reduced. To explain the observed pattern, we use the SU(2) coherent states to analytically connect the eigenfunctions with the geometrical rays. With the SU(2) coherent state, the observe vector pattern is completely reconstructed and the vector vortex lattice is manifest.

In this investigation, we fabricate square shaped VCSELs with large aperture and measure near-field transverse patterns. The size of the oxide aperture is $40 \times 40\ \mu m^2$. The device structure of these oxide-confined VCSELs is similar to that described by Ref. [14]. The effective cavity length between two distributed feedback reflectors is designed to have the emission wavelength around $\lambda_z = 799.5$ nm. The near-field patterns are measured with a CCD camera (Coherent, Beam-Code) and an optical setup similar to that described in Ref. [14]. An optical spectrum analyzer (ADVANTEST Q8347) is used to monitor the spectral information of the laser.

The performance of the VCSEL device is measured at a temperature around 0 °C. It is found that near lasing threshold the transverse pattern is linearly polarized, but the polarization is not the same for different points of the transverse plane. In other words, the observed pattern is a vector pattern formation and its polarization is position dependent. The measurement of the optical spectrum verifies that the observed transverse pattern is phase synchronized to a single frequency at 795 nm. Even though a single-frequency high-order transverse pattern has been observed in VCSELs [14], it is usually a scalar pattern formation; i.e., the polarization is always the same for all points of the transverse plane. The basic requirement for a vector polarization pattern is that the orthogonal polarization modes with different spatial patterns are phase synchronized to a common frequency. The polarization modes normally are frequency degenerate; however, strain or electric field induced birefringence may lift the degeneracy to the order of $\Delta\lambda = 0.05$ nm [15]. We find that about half the present fabricated devices can have the property of the frequency locking between the polarization modes. Therefore, we speculate that the frequency locking between the polarization modes is subject to the degree of birefringence effect. Figures 1(a) and 1(b) show the polarization resolved near-field patterns in the 45° and −45° direction, respectively. The polarization angle is referring to the [110] direction of the (001)-GaAs crystal. It can be seen that near-field components of orthogonal polarizations have different pattern structures. Since the orthogonally polarized near-field patterns are phase synchronized to a common frequency, the orthogonally polarized components can mutually interfere to lead to a greatly different pattern in the polarization resolved near-field image, as shown in Fig. 1(c) for 0° polarization.

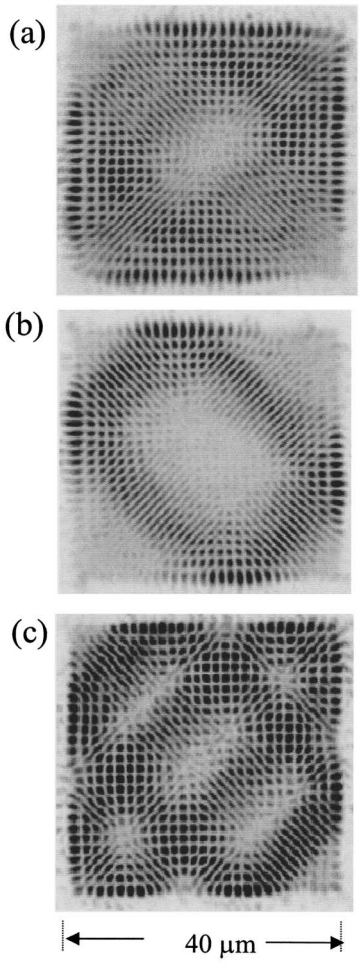

FIG. 1. Experimental polarization resolved pattern emitted from the VCSEL device near lasing threshold: (a) −45° polarization; (b) +45° polarization; (c) 0° polarization.

In order to understand the observed transverse patterns, we consider the large aperture VCSEL to be a planar waveguide with a dominant wave vector along the vertical direction. According to the waveguide theory [16], the electromagnetic fields with a predominant z direction of propagation can be approximated as $\vec{E}(x, y, z, t) = \vec{E}(x, y)e^{i(\beta z-\omega t)}$, where ω is the angular frequency and β is the propagation constant along the z direction. After separating the z dependence in Maxwell equation, we are left with a two-dimensional (2D) Helmholtz equation: $(\nabla_t^2 + k_t^2)\vec{E}(x, y) = 0$, where $k_t^2 = (\omega/c)^2 - \beta^2$, and c is the wave speed. Since the photons will experience total reflection at the lateral oxide walls, the extension of the evanescent field is reduced. Therefore, we approximate the wave function to obey the condition of $\vec{E}(x, y) = 0$ on the boundary.

As is well known, the eigenfunction for the Helmholtz equation with a square rigid boundary is given by

$$\psi_{m,n}(x, y) = \frac{2}{a}\sin\left(\frac{m\pi x}{a}\right)\sin\left(\frac{n\pi y}{a}\right), \tag{1}$$

$$k_t^2 = \left(\frac{m\pi}{a}\right)^2 + \left(\frac{n\pi}{a}\right)^2. \tag{2}$$

Since the functional form of the present resonator is similar to the 2D Helmholtz equation, it is possible to describe $\vec{E}(x, y)$ with the eigenfunctions $\psi_{m,n}(x, y)$. However, the subtle solution in Eq. (1) cannot account for the present observed pattern localized on the geometrical trajectories. Recently, Pollet *et al.* [17] demonstrated that the wave function of the SU(2) coherent state for the 2D quantum harmonic oscillation is well localized on the corresponding classical elliptical trajectory. As in the Schwinger representation of the SU(2) algebra [18], SU(2) transverse mode functions for a square planar waveguide are expressed as [19]

$$\Psi_N(x, y; \phi) = \left(\frac{2}{a}\right)\frac{1}{2^{N/2}}\sum_{K=0}^{N}\binom{N}{K}^{1/2} e^{iK\phi}\sin\left[(K+1)\frac{\pi x}{a}\right] \times \sin\left[(N-K+1)\frac{\pi y}{a}\right], \tag{3}$$

where the parameter ϕ is related to the wall positions of specular reflection points and the quantity $\binom{N}{K}$, which equals $N!/[K!(N-K)!]$ is a binomial coefficient. The index N is related to the average value of $\langle k_t^2\rangle$. Experimentally, the value of N is determined by the detuning between the longitudinal cavity resonance and the gain emission frequency. The relationship between the parameter ϕ and the periodic orbits can be understood by using the identity of $\sin z = (e^{iz} - e^{-iz})/2i$ to rewrite Eq. (3) and applying the property of the *Dirichlet kernel*. Numerical calculations show that the behavior of $|\Psi_N(x, y; \phi)|^2$ agrees very well with the geometrical trajectory (classical periodic orbit), as shown in Fig. 2. To our knowledge, it is original to use the eigenfunctions of the Helmholtz equation with a square rigid boundary to describe the VCSEL transverse modes.

The wave function given in Eq. (3) represents a traveling-wave property. The standing-wave representations can be obtained by using $\Psi_N(x, y; \phi) \pm \Psi_N^*(x, y; \phi)$. Although the wave function representation in Eq. (3) consists of $N + 1$ eigenstates, numerical analyses reveal that a superposition of only a few eigenstates is already sufficient to result in the localization on the classical trajectory. To include this property, the partially coherent states for the standing wave can be expressed as

$$\Psi_{N,M}^c(x, y; \phi) = \frac{(2/a)}{\left[\sum_{K=q}^{N-q}\binom{N}{K}\cos^2 K\phi\right]^{1/2}}\sum_{K=q}^{N-q}\binom{N}{K}^{1/2}(\sin K\phi)\sin\left[(K+1)\frac{\pi x}{a}\right]\sin\left[(N-K+1)\frac{\pi y}{a}\right], \tag{4}$$

and

$$\Psi^{s}_{N,M}(x, y; \phi) = \frac{(2/a)}{\left[\sum_{K=q}^{N-q}\binom{N}{K}\cos^2 K\phi\right]^{1/2}} \sum_{K=q}^{N-q}\binom{N}{K}^{1/2} (\sin K\phi) \sin\left[(K+1)\frac{\pi x}{a}\right] \sin\left[(N-K+1)\frac{\pi y}{a}\right] \tag{5}$$

where the index $M = N - 2q + 1$ represents the number of eigenstates used in the wave function. Using Eqs. (4) and (5) to fit the experimental result, it is found that $E_{-}(x, y) = \Psi^{s}_{53,4}(x, y; -0.38\pi)$ and $E_{+}(x, y) = \Psi^{c}_{53,8}(x, y; 0.59\pi)$, where $E_{-}(x, y)$ and $E_{+}(x, y)$ are the field distribution for the observed patterns in the $-45°$ and $+45°$ direction, respectively. In terms of $E_{-}(x, y)$ and $E_{+}(x, y)$, the field distribution for the observed pattern can be expressed as

$$\vec{E}(x, y) = E_x(x, y)\vec{a}_x + E_y(x, y)\vec{a}_y, \tag{6}$$

where

$$E_x(x, y) = [\Psi^{c}_{53,8}(x, y; 0.59\pi) + \Psi^{s}_{53,4}(x, y; -0.38\pi)]/\sqrt{2}, \tag{7}$$

and

$$E_y(x, y) = [\Psi^{c}_{53,8}(x, y; 0.59\pi) - \Psi^{s}_{53,4}(x, y; -0.38\pi)]/\sqrt{2}. \tag{8}$$

The polarization resolved near-field patterns shown in Fig. 1 are numerically reconstructed by $|E_{-}(x, y)|^2$, $|E_{+}(x, y)|^2$, and $|E_x(x, y)|^2$, as depicted in Fig. 3. The excellent agreement between the experimental and reconstructed patterns evidences that the oxide-confined VCSEL cavity can be considered as a planar waveguide. Moreover, it is greatly important to note that the eigenstates used to expand the observed transverse patterns are not exactly degenerate but nearly degenerate. This result indicates that the spontaneous transverse mode locking within almost-degenerated modes plays an important mechanism in the laser pattern formation [20]. Another intriguing point is that the observed patterns of Fig. 2(b) are similar to the diamond-shape scar that has been discussed extensively in the wave functions of ballistic quantum dots [21,22].

With the analytical function given in Eqs. (6)–(8), the polarization pattern of the observed mode is illustrated in Figs. 4(a) and 4(b) for global view and zoom-in view, respectively. The vector vortex lattice can be clearly seen from the zoom-in view. To our knowledge, the preset

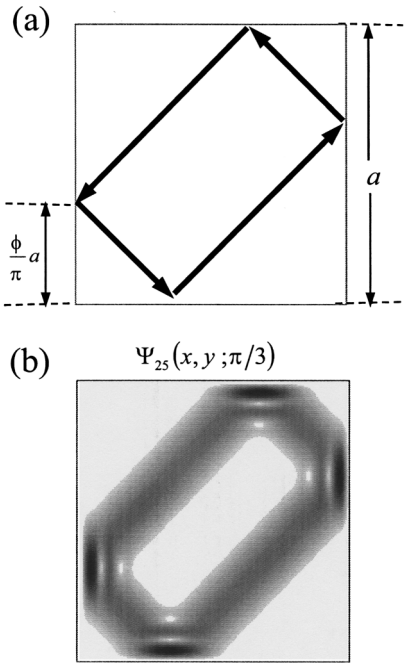

FIG. 2. (a) A typical ray trajectory. (b) The wave pattern $|\Psi_N(x, y; \phi)|^2$ from Eq. (3) for $N = 25$.

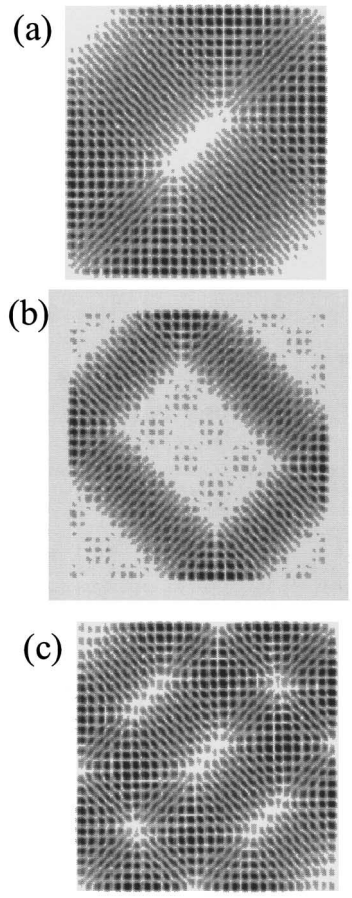

FIG. 3. Theoretically reconstructed patterns for the results shown in Fig. 1, calculation with Eqs. (6)–(8).

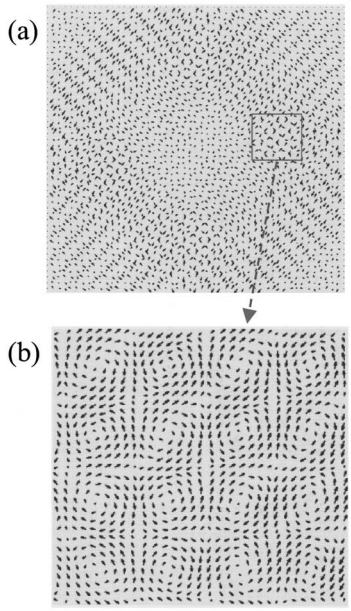

FIG. 4. Numerically calculated polarization planes for the observed pattern (a) global view; (b) zoom-in view.

experiment provides the first observation of a vector vortex lattice in an isotropic laser. Although the mode order may change with changing the temperature, the basic pattern formation does not change. Moreover, the observed pattern retains its identity even when the pump current increases about $1 \sim 3$ mA. In other words, the observed pattern is generic and structurally stable.

In summary, a vector polarization pattern has been observed in an isotropic microcavity laser. The observed transverse patterns are analytically reconstructed by using the partially coherent states. With the analytical function, the formation of vector vortex lattices in the observed pattern is clearly shown.

The authors gratefully acknowledge various VCSEL devices from TrueLight Corporation. The authors also thank the National Science Council for their financial support of this research under Contract No. NSC-91-2112-M-009-030.

*Author to whom correspondence should be addressed.
Permanent address: Department of Electrophysics, National Chiao Tung University, 1001 TA Hsueh Road, Hsinchu, Taiwan, 30050.
Electronic address: yfchen@cc.nctu.edu.tw

[1] G. Blatter, M.V. Feigelman, and V. B. Geshkenbein, Rev. Mod. Phys. **66**, 1125 (1994).
[2] R. E. Prange and M. Girvin, *The Quantum Hall Effect* (Springer-Verlag, Berlin, 1990), 2nd ed.
[3] F. Dalfovo, S. Giorgin, L. P. Pitaevskii, and S. Stringari, Rev. Mod. Phys. **71**, 463 (1999).
[4] J. F. Nye and M.V. Berry, Proc. R. Soc. London A **336**, 165 (1974).
[5] M.V. Berry, *Physics of Defects*, Proceedings of the Les Houches Summer School, Session XXXV (North-Holland, Amsterdam, 1981), p. 453.
[6] M.V. Berry, Proc. SPIE **3487**, 1 (1998).
[7] C. Tamm, Phys. Rev. A **38**, 3960 (1988).
[8] Y. F. Chen and Y. P. Lan, Phys. Rev. A **64**, 063807 (2001).
[9] L. Gil, Phys. Rev. Lett. **70**, 162 (1992).
[10] L. M. Pismen, Physica (Amsterdam) **73D**, 244 (1994).
[11] J. F. Nye and J.V. Hajnal, Proc. R. Soc. London A **409**, 21 (1987).
[12] C. Taggiasco, R. Meucci, M. Ciofini, and N. B. Abraham, Opt. Commun. **133**, 507 (1997).
[13] F. Prati, G. Tissoni, M. S. Miguel, and N. B. Abraham, Opt. Commun. **143**, 133 (1997).
[14] S. P. Hegarty, G. Huyet, J. G. McInerney, and K. D. Choquette, Phys. Rev. Lett. **82**, 1434 (1999).
[15] M. P. van Exter, A. K. Jansen van Doorn, and J. P. Woerdman, Phys. Rev. A **56**, 845 (1997).
[16] J. D. Jackson, *Classical Electrodynamics* (Wiley, New York, 1975), Chap. 8.
[17] J. Pollet, O. Méplan, and C. Gignoux, J. Phys. A **28**, 7282 (1995).
[18] J.V. Schwinger, in *Quantum Theory of Angular Momentum*, edited by L. C. Biederharn and H. Van Dam (Academic, New York, 1965).
[19] V. Bužek and T. Quang, J. Opt. Soc. Am. B **6**, 2447 (1989).
[20] L. A. Lugiato, C. Oldano, and L. M. Narducci, J. Opt. Soc. Am. B **5**, 879 (1988).
[21] R. Akis, D. K. Ferry, and J. P. Bird, Phys. Rev. Lett. **79**, 123 (1997).
[22] I.V. Zozoulenko and K. F. Berggren, Phys. Rev. B **56**, 6931 (1997).